Journal of Hydrology 533 (2016) 461–472

Contents lists available at ScienceDirect

Journal of Hydrology

journal homepage: www.elsevier.com/locate/jhydrol

Impacts of biochar concentration and particle size on hydraulic conductivity and DOC leaching of biochar–sand mixtures

Zuolin Liu [a,*], Brandon Dugan [a], Caroline A. Masiello [a,b], Rebecca T. Barnes [a,1], Morgan E. Gallagher [a,2], Helge Gonnermann [a]

[a] Department of Earth Science, Rice University, 6100 Main St., MS 126, Houston, TX 77005, United States
[b] Department of Chemistry, Rice University, 6100 Main St., MS 60, Houston, TX 77005, United States

ARTICLE INFO

Article history:
Received 23 December 2014
Received in revised form 25 November 2015
Accepted 3 December 2015
Available online 17 December 2015
This manuscript was handled by Peter K. Kitanidis, Editor-in-Chief, with the assistance of Nunzio Romano, Associate Editor

Keywords:
Biochar
Hydraulic conductivity
Particle size
Dissolved organic carbon

SUMMARY

The amendment of soil with biochar can sequester carbon and alter hydrologic properties by changing physical and chemical characteristics of soil. To understand the effect of biochar amendment on soil hydrology, we measured the hydraulic conductivity (K) of biochar–sand mixtures as well as dissolved organic carbon (DOC) in leachate. Specifically, we assessed the effects of biochar concentration and particle size on K and amount of DOC in the soil leachate. To better understand how physical properties influenced K, we also measured the skeletal density of biochars and sand, and the bulk density, the water saturation, and the porosity of biochar–sand mixtures. Our model soil was sand (0.251–0.853 mm) with biochar rates from 2 to 10 wt% (g biochar/g total soil × 100%). As biochar (<0.853 mm) concentration increased from 0 to 10 wt%, K decreased by 72 ± 3%.

When biochar particle size was equal to, greater than, and less than particle size of sand, we found that biochar in different particle sizes have different effects on K. For a 2 wt% biochar rate, K decreased by 72 ± 2% when biochar particles were finer than sand particles, and decreased by 15 ± 2% when biochar particles were coarser than sand particles. When biochar and sand particle size were comparable, we observed no significant effect on K. We propose that the decrease of K through the addition of fine biochar was because finer biochar particles filled spaces between sand particles, which increased tortuosity and reduced pore throat size of the mixture. The decrease of K associated with coarser biochar was caused by the bimodal particle size distribution, resulting in more compact packing and increased tortuosity.

The loss of biochar C as DOC was related to both biochar rate and particle size. The cumulative DOC loss was 1350% higher from 10 wt% biochar compared to pure sand. This large increase reflected the very small DOC yield from pure sand. In addition, DOC in the leachate decreased as biochar particle size increased. For all treatments, the fraction of carbon lost as DOC ranged from 0.06 to 0.18 wt% of biochar. These experiments suggest that mixing sandy soils with biochar is likely to reduce infiltration rates, holding water near the surface longer with little loss of biochar-derived carbon to groundwater and streams.
© 2015 Elsevier B.V. All rights reserved.

1. Introduction

Biochar amendment of soil has been proposed for carbon (C) sequestration (Molina et al., 2009; Woolf et al., 2010) and for improving soil productivity (Liu et al., 2013). Biochar may also improve soil performance by altering soil physical characteristics such as porosity (ϕ), bulk density (ρ_b), hydraulic conductivity (K), and water holding capacity (Githinji, 2013; Herath et al., 2013; Streubel et al., 2011; Tryon, 1948) and by changing soil chemical properties including pH, cation exchange capacity, and nutrient availability (Deal et al., 2012; Liu et al., 2012; Major et al., 2009).

The rate of water movement through soil is important for infiltration, delivery of water to plant roots, and flow of water to streams, groundwater, and oceans (Klute, 1986). Hydraulic conductivity is a measurement of the ease of water movement through porous media and is related to other soil properties (e.g., effective porosity, pore throat size, tortuosity, and hydrophobicity) and fluid properties (e.g., fluid saturation (S), viscosity, and density) (Freeze and Cherry, 1979).

Previous studies showed that amending soil with biochar can either increase or decrease K (Barnes et al., 2014; Brockhoff et al., 2010; Githinji, 2014; Herath et al., 2013). Using the falling head

* Corresponding author. Tel.: +1 713 348 2113; fax: +1 713 348 5214.
E-mail address: zl17@rice.edu (Z. Liu).
[1] Present address: Environmental Program, Colorado College, Colorado Springs, CO, United States.
[2] Present address: Rm. 3307, French Family Science Center, Duke University, NC, United States.

http://dx.doi.org/10.1016/j.jhydrol.2015.12.007
0022-1694/© 2015 Elsevier B.V. All rights reserved.

method to determine K, Barnes et al. (2014) showed that adding 10 wt% biochar (g biochar/g total soil × 100%) can decrease the K of sand by 92%, decrease the K of organic soil by 67%, but increase the K of clay by 328%. Githinji (2014) conducted cumulative infiltration experiments using an infiltrometer and documented a linear decrease in K of a sandy loam with an increasing biochar rate from 0% to 100% by volume. From constant head experiments, Brockhoff et al. (2010) observed that K of sand-based turf grass root zones decreased from 58.9×10^{-5} to 4.6×10^{-5} m/s as biochar rate increased from 0% to 25% by volume. In another series of constant head experiments, Herath et al. (2013) documented increases in K of Alfisols by 50%, 32% and 139% when adding unpyrolyzed corn stover, 350 °C corn stover biochar, and 550 °C corn stover biochar at 7.18 t C/ha, respectively. Herath et al. (2013) also showed a similar increase in K (41%) by adding 350 °C corn stover biochar at 7.18 t C/ha to an Andisol. Additionally, Herath et al. (2013) found that the increase in K correlated with an increase of interparticle macropore volume. These changes in hydraulic conductivity through biochar are sometimes intended to have a lasting effect on soil water movement (Herath et al., 2013) and thus affect the hydrologic cycle.

Porosity may play a role in how K changes in biochar-amended soils as pores can allow water migration and can change the tortuosity of flow paths. Increased porosity in soils after biochar amendment results from pores inside biochar particles (ϕ_{intra}, intraporosity) and from pores between biochar and soil particles (ϕ_{inter}, interporosity) (Masiello et al., 2015). Depending on the pore size, the pore connectivity, and the hydrophobicity of the particle surface, these two types of porosity may or may not be effective for water flow or water storage. When pores are connected, water moves faster in larger pores than in smaller pores and thus larger pores dominate water flow through porous media. Meanwhile, biochar particles can have high initial hydrophobicity if they are produced at low temperatures (<400 °C) (Kinney et al., 2012). Hydrophobic biochar has positive water entry pressure (Wang et al., 2000), which means that an applied pressure is required for water to enter intrapores. If the hydrostatic pressure is less than the water entry pressure, water will not enter these intrapores, therefore reducing their effectiveness of water flow and water storage. Amending soil with biochar will likely change porosity, pore size, pore connectivity, and hydrophobicity of soil because of the dual porosity of the system, changes in the particle size distribution, and hydrophobicity of the biochar. Combined, these changes can affect the hydraulic conductivity.

Feedbacks likely exist between the effects of biochar on soil water and carbon. The ability of biochar to sequester C can be affected by the mobility and retention of biochar within the soil matrix (Glaser et al., 2002; Zhang et al., 2010). Mobilization of biochar could occur via erosion through runoff (Glaser et al., 2002; Major et al., 2010; Rumpel et al., 2006, 2009), microbial and abiotic decay (Czimczik and Masiello, 2007; Foereid et al., 2011; Kuzyakov et al., 2009; Zimmerman, 2010), or vertical movement deeper into the soil profile or into groundwater, either via leachate (Hockaday et al., 2006; Major et al., 2010) or as particulate organic carbon (Lehmann and Joseph, 2009). Its ultimate fate can include discharge into the ocean (Dittmar et al., 2012; Jaffé et al., 2013).

Amending soil with biochar may change soil K, thus altering the partitioning of precipitation between infiltration and surface runoff. If that is the case, the transport of biochar (with surface runoff or downward into groundwater) could be affected. In addition, the increased transport of pyrogenic DOC to depth in soils could increase soil C storage as deeper soil C is more protected from decomposition (Schaetzl, 2002). Therefore it is important to investigate the influence of biochar on K as well as biochar C movement as DOC leachate to understand the coupled effects of biochar on carbon and water in soils.

We hypothesized that adding biochar into soil may affect soil K by changing pore characteristics and soil hydrophobicity, and may also introduce DOC into groundwater. To better characterize the impacts of biochar on these soil properties, we quantitatively investigated the K of biochar–sand mixtures and the concentration of DOC in the leachate collected during falling head experiments in the lab. Measuring changes in K associated with biochar rate (biochar% by dry weight) and biochar particle size allowed us to better understand the effects of biochar on water movement in an idealized coarse soil (sand). We also measured skeletal density of biochars (ρ_{sb}) and sand (ρ_{ss}), bulk density (ρ_b), and calculated ϕ, and S (percent of pore volume occupied by water) of our biochar–sand mixtures to help understand the physical mechanisms that may cause changes in K and in DOC leaching.

2. Materials and methods

2.1. Biochar production

Heat transport occurs differently in coarser biochar particles compared to finer biochar particles, confounding biochar chemistry and particle size if feedstock is ground after pyrolysis. To avoid this we pre-ground all biomass feedstocks to a uniform size prior to pyrolysis. The biochar particle sizes were different in our two experiments (concentration experiment and particle size experiment). For the concentration experiment we ground mesquite (*Prosopis* sp.) wood feedstock into particles <0.853 mm, and for the particle size experiment we produced biochar from feedstock particles 1.70–2.00 mm (Table 1). Biochar in the particle size experiment were further ground after production (see Section 2.3).

To produce biochar we placed 45 g of ground mesquite into a stainless steel crucible and packed each batch of ground mesquite to the same volume to minimize variation in heating rates between batches. We covered the steel crucible with ceramic fiber insulation and buried it inside a larger stainless steel, open-top vessel using approximately 9 kg of silica sand to allow uniform heat conduction (Kinney et al., 2012). The vessel was heated in a muffle furnace at a rate of 5 °C/min until the furnace temperature reached 400 °C. We set the furnace to hold at 400 °C for 4 h and then allowed the biochar to cool down in the absence of oxygen for a minimum of 16 h. The general properties of biochars used in this study are shown in Table 1.

We measured the biochar mass yields immediately after pyrolysis, and found the mass yield to be constant at 44 wt% (no variation within the error of the balance used to measure mass, ±0.001 kg). Biochar was stored in sealed glass jars until it was used in our experiments. Because biochar may absorb water after being exposed to air, we oven-dried all biochars samples at 60 °C for 72 h prior to use to remove any water absorbed during storage. We massed biochar samples immediately after drying to insure an accurate dry mass value.

2.2. Biochar characterization

We collected basic information on the biochar including one replicate of measurement for ash content, pH, and electrical conductivity (EC), and three replicates of measurements for hydrophobicity, %C, %N, and %H. (Table 1). We placed a portion of oven-dried biochar in a ceramic crucible and heated at 750 °C for 6 h to measure ash content. To measure the EC and pH we first mixed a 1:20 (w:v) suspension of biochar: Milli-Q water (18.2 MΩ-cm, PURELAB® Ultra Laboratory Water Purification Systems, SIEMENS, Germany) on a shaker for 1.5 h (IBI, 2013). We measured the surface hydrophobicity of biochar using the molarity of ethanol drop (MED) test (Doerr, 1998). We reported the range of ethanol

Table 1
General properties of silica sand and biochar used in this study. Values and error bars were the average and standard deviation of three replicates conducted for each treatment.

Properties	Data
Silica sand	
Particle size (mm)	0.251–0.853
pH	7.06
Electric conductivity (μs/cm)	77
MED index	0
%C	0.14 ± 0.05
%H	NA
%N	NA
Biochar production	
Feedstock	Mesquite
Heating rate (°C/min)	5
Heating duration (h)	4
Pyrolysis temperature (°C)	400
Mass yield (wt%)	44.4
Biochar in concentration experiment	
Mesquite feedstock particle size before pyrolysis (mm)	<0.853
Biochar particle size used in experiment (mm)	<0.853
Biochar rate (wt%)	0, 2, 4, 6, 8 and 10
Ash content (wt%)	5.06
pH	7.95
Electric conductivity (μs/cm)	238
MED index	3–5
%C	68 ± 1
%H	3.0 ± 0.1
%N	0.76 ± 0.01
MED index of biochar–sand mixtures	0
Biochar in particle size experiment	
Mesquite feedstock particle size before pyrolysis (mm)	1.70–2.00
Biochar particle size used in experiment (mm)	<0.251, 0.251–0.853, 0.853–2.00
Biochar rate (wt%)	0 and 2
Ash content (wt%)	4.26
pH	7.41
Electric conductivity (μs/cm)	110
MED index	3–5
%C	73.0 ± 0.4
%H	3.2 ± 0.1
%N	0.74 ± 0.01
MED index of biochar–sand mixtures	0

concentrations (MED index) at which the sample starts absorbing the ethanol solution within three seconds. We measured the %C, %N, and H% by mass of the pure biochar using a Costech ECS4010 elemental analyzer (within error of ±1%, ±0.1% and ±0.01% for %C, %N, and H%, respectively).

2.3. Sample preparation

We wet-sieved silica sand (Pavestone, USA) to a particle size between 0.251 mm (U.S. Std. No. 60 mesh) and 0.853 mm (U.S. Std. No. 20 mesh) to obtain a narrow particle size range without defining particle size distribution of sand. The sieved sand was heated for at least 72 h at 60 °C before experiments to remove any moisture. We mixed biochar with sand in aluminum jars by hand shaking to achieve homogeneous samples. In concentration experiments, the biochar (dry-sieved to particle size <0.853 mm) rates were 0 wt%, 2 wt%, 4 wt%, 6 wt%, 8 wt%, and 10 wt.%, which are equal to 0, 22, 44, 66, 88 and 111 Mg C/ha for an application depth of 12.0 ± 2.0 cm (the average length of our samples with 0–10 wt% biochar). In particle size experiments, the biochar (particle size pre-pyrolysis: 1.70–2.00 mm) was ground from one batch and dry-sieved it into three size ranges (fine: <0.251 mm, medium: 0.251–0.853 mm, coarse: 0.853–2.00 mm) to obtain biochar finer than sand, the same as sand, and coarser than sand. The biochar amendment rate was 2 wt%, which is equal to 22 Mg C/ha for an application depth of 10.4 ± 0.4 cm (the average length of our samples with 2 wt% biochar in particle size experiments). Three replicates of each treatment resulted in a total of 18 samples in concentration experiments and 12 samples in particle size experiments (Table 1).

We explored high biochar rates, up to 10 wt%, to detect any effects beyond 2 wt%. This allowed us to derive relationships between biochar rate, K, and DOC leaching. The upper limit (10 wt%) was selected based on previous experiments conducted that showed 10 wt% biochar has an effect on soil K and C export (Barnes et al., 2014).

2.4. Experimental setup and procedures

Some method modifications were necessary to measure the K in our biochar–sand mixtures and DOC concentration in leachate from these mixtures. The hydraulic conductivity of our sand (wet-sieved, 0.251–0.853 mm) was greater than 1×10^{-5} m/s (Fig. 1). For K values of this magnitude, the constant head method was recommended to measure K (ASTM International, 2006); however, this method did not allow us to measure DOC concentration quantitatively in the leachate. To address this we compared constant head and falling head K values for our sand, and confirmed that both methods gave the same hydraulic conductivity ($p = 0.3796$, p value was obtained by two-tailed t-tests, differences are deemed significant at a p-value less than 0.05, Fig. 1). The use of falling head tests allowed us to measure K in our biochar–sand mixtures and to easily collect and analyze leachate quantitatively. Falling head experiments additionally allowed rapid completion of multiple replicates. Although distilled water is not recommended as a permeant fluid because it can lower the hydraulic conductivity of clayey soils (ASTM International, 2010), we used Milli-Q water as the permeant fluid because: (1) sand was unlikely to swell in response to wetting, thus using distilled water has lower influence on K for sand than for clay; and (2) Milli-Q water provided a blank to address how DOC in the leachate is produced from biochar C. We de-aired permeant fluid under vacuum prior to experiments to remove air bubbles in water.

We constructed falling head columns to measure K (see Barnes et al., 2014). Before adding the biochar–sand mixture evenly to the bottom of a clear plastic cylindrical column (0.0198 m inner radius, 0.25 m height), we fastened a piece of 54 μm polyester mesh (Part

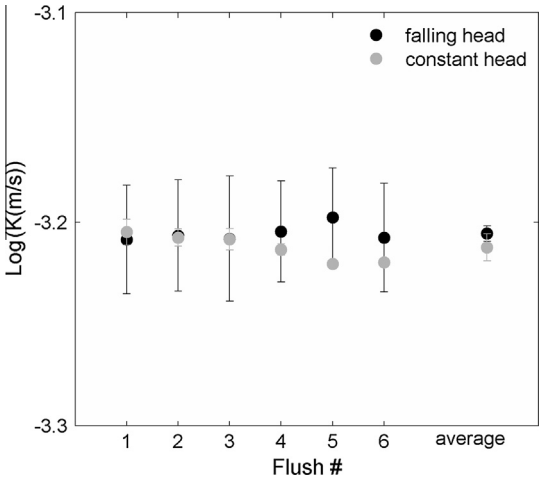

Fig. 1. The hydraulic conductivity (K) of sand (0.251–0.853 mm) measured by falling head (black dots) method and constant head (gray dots) method ($p = 0.3796$) were statistically identical.

No.: CMY-0054-10YD, Small parts, FL) to the bottom of the column to allow water flow while preventing soil loss. We attached measuring tape (S.E. Rose Co., TX) along the height of each column to facilitate accurate measurements of sample length and hydraulic head (h). To fill the sample columns, we gently poured the biochar–sand mixture into the columns, we then placed a piece of 54 μm polyester mesh on the top of the sample and then a porous, permeable stone (cleaned using a Branson 1510 Ultrasonic Cleaner in Milli-Q water to avoid contamination) to confine the sample surface and to allow even distribution of water through sample. The last step was to load each sample with 4.54 kg mass to allow compaction under a constant load. We monitored sample length until it did not change; this was recorded as the sample length (L, ranged from 0.097 to 0.148 m). We then placed the base of each column into a plastic cup and filled the cup with Milli-Q water to allow the water to rise into the sample from bottom to top all at once. Each sample was stored in the water-filled saturation cup for two days without drainage to insure saturation.

2.4.1. Hydraulic conductivity

We allowed free, gravity-driven drainage of water through the samples until water level was ~0.005 m above the top of the sample and collected the first leachate (Flush 0) for DOC analysis. We then poured 300 ml of Milli-Q water into each column and recorded the hydraulic head until the water level was ~0.005 m above the top of the sample. We used this approach to conduct six flushes (Flush 1–6) for each sample, each flush right after the previous one to prevent any drying between flushes. We collected leachate from each flush for DOC analysis. We monitored the head change over time to determine K for each flush (Klute, 1986) by Eq. (1).

$$K = \ln(h_2/h_1)L/\Delta t \quad (1)$$

where Δt was time elapsed (s), h_1 was initial head (0.25 m) from water surface to sample bottom, and h_2 was final head (varying between 0.24 and 0.19 m). This equation defines the hydraulic conductivity for saturated samples. For consistency we used Eq. (1) and report water saturation (S) for all samples (Eq. (3)). The falling head experiments were conducted following the protocol as described in ASTM standard D5085 (ASTM International, 2010).

2.4.2. Skeletal density, bulk density, and saturation

Pores inside plant-derived biochars (intrapores) are bimodal in size distribution (Sun et al., 2012), and these pores may or may not be connected. Even when pores are connected, nanometer-scale pores may be too small to permit water entry (Brewer et al., 2014). To make a first assessment of the pore connectivity, we measured the skeletal densities of the biochar in different particle sizes and sand used in the falling head experiments using helium (He) pycnometry (AccuPyc II 1340, Micromeritics Instrument Corporation, USA) (Table 2). Helium pycnometry measured the volume of the biochar skeleton by measuring the volume of He displaced; the mass of the biochar sample was divided by this volume to provide a skeletal density of biochar (ρ_{sb}) (Brewer et al., 2014).

Using sample length, inner radius of the column (r = 0.0198 m) and total sample mass (M = 0.2 kg), we calculated the dry bulk density (ρ_b) of each biochar–sand mixture (Table 3) using Eq. (2).

$$\rho_b = \frac{M}{\pi r^2 L} \quad (2)$$

After we finished six flushes and water surface was no longer above the top of the sample, we massed the wet sample (M_t). We then oven-dried each sample until its mass did not change. We then calculated S (Eq. (3), Table 3), which is the percent of pore space occupied by water.

$$S = \frac{(M_t - M_d)/\rho_w}{\pi r^2 L - M_s/\rho_{ss} - M_{bc}/\rho_{sb}} \times 100\% \quad (3)$$

where M_d was the oven-dried sample mass (kg) and ρ_w is density of water (1000 kg/m^3), M_s was mass of sand (0.2 × (1-biochar%) kg), ρ_{ss} was skeletal density of sand (kg/m^3, Table 2), M_{bc} was mass of biochar (0.2 × biochar% kg), and ρ_{sb} was skeletal density of biochar (kg/m^3, Table 2). The dry mass was very close to the pre-experiment mass (0.2 kg) with 0.4 ± 0.2% mass loss. If S = 100%, all pores were filled with water and the sample was fully saturated; if S < 100%, the sample was partially saturated (pores are partially filled by water and partially filled by air).

2.4.3. Total porosity, effective porosity, interporosity, and intraporosity

Porosity is the fraction of pore volume per total sample volume (pores plus solids). In this study, the total porosity (ϕ_T) of the biochar–sand mixture was the sum of intraparticle and interparticle porosity and was defined by the volume fraction that could be invaded by He. We calculated ϕ_T (Eq. (4), Table 3) using skeletal density data.

$$\phi_T = \frac{\pi r^2 L - M_s/\rho_{ss} - M_{bc}/\rho_{sb}}{\pi r^2 L} \quad (4)$$

The total porosity measured by He may be larger than the porosity accessible by water, because water is a larger molecule than helium. To examine the porosity accessible by water, we also calculated effective porosity (ϕ_{eff}, Eq. (5)). Effective porosity is equal to the volume of pores accessible by water (V_{ep}) divided by total sample volume (V_T, = $\pi r^2 L$).

$$\phi_{eff} = \frac{V_{ep}}{V_T} \quad (5)$$

Table 2
Skeletal density (kg/m^3) of silica sand (ρ_{ss}) and biochar (ρ_{sb}) used in this study. Values and error bars were the average and standard deviation of three replicates conducted for each treatment.

Particle size	Silica sand	Biochar in concentration experiment	Biochar in particle size experiment
<0.251 mm	–	–	1477 ± 2
<0.853 mm	–	1500 ± 10	–
0.251–0.853 mm	2660 ± 20	–	1452 ± 5
0.853–2.00 mm	–	–	1430 ± 2

Table 3
Bulk density (ρ_b) and water saturation (S) after the final flush of each treatment in this study. Values and error bars were the average and standard deviation of three replicates conducted for each treatment, respectively.

Biochar particle size (mm)	Biochar rate (wt%)	ρ_b (kg/m^3)	S (%)
Concentration experiment			
–	0	1620 ± 30	102 ± 3
<0.853	2	1450 ± 10	96 ± 1
<0.853	4	1340 ± 20	90 ± 2
<0.853	6	1280 ± 20	87 ± 3
<0.853	8	1200 ± 10	87 ± 4
<0.853	10	1110 ± 10	82 ± 5
Particle size experiment			
–	0	1660 ± 40	105 ± 5
<0.251	2	1540 ± 10	88 ± 4
0.251–0.853	2	1520 ± 20	101 ± 1
0.853–2.00	2	1570 ± 10	99 ± 3

The volume of pores accessible by water (effective pores) equaled total sample volume minus volume of sand particles (V_s) and volume of biochar solids (V_{bc}, including pores that were inaccessible to water) (Eq. (6)).

$$V_{ep} = V_T - V_s - V_{bc} \tag{6}$$

For sand, the volume of sand particles equaled to the mass of sand divided by the density of sand (Eq. (7)).

$$V_s = \frac{M_s}{\rho_{ss}} \tag{7}$$

Below we discuss three means of estimating solid volume of biochar based on the accessibility of the internal pores to water.

(a) If all biochar internal pores were accessible to water and V_{ep} was the volume of interpores plus intrapores, then V_{bc} was the volume of biochar skeleton measured by helium pyconometry (Eq. (8) and Fig. 2a). In this case, effective porosity equaled total porosity.

$$V_{bc} = \frac{M_{bc}}{\rho_{sb}} \tag{8}$$

(b) If all biochar internal pores were not accessible to water and V_{ep} was the volume of interpores only in the mixture, then V_{bc} was the volume of biochar skeleton plus biochar internal pores (Eq. (9) and Fig. 2b). In this scenario, effective porosity equaled interporosity.

$$V_{bc} = \frac{M_{bc}}{\rho_{eb}} \tag{9}$$

where ρ_{eb} was the envelope density of biochar particle, $\rho_{eb} = (1 - \phi_{bc})\rho_{sb}$; ϕ_{bc} was internal porosity of biochar (Brewer et al., 2014).

(c) Intermediate between scenarios (a) and (b), where some fraction (f, ranges from 0 to 1) of biochar internal pores were accessible to water. In this case, V_{ep} was volume of interpores plus accessible intrapores (Fig. 2c). Then V_{bc} was volume of biochar skeletal plus non-accessible biochar internal pores (Eq. (10)). In this scenario, effective porosity was the sum of interporosity and a fraction of intraporosity.

$$V_{bc} = \frac{M_{bc}}{\rho_{sb}} + \frac{M_{bc}}{\rho_{eb}}\phi_{bc}(1-f) \tag{10}$$

If we substitute $(1 - \phi_{bc})\rho_{sb}$ for ρ_{eb}, then

$$V_{bc} = \frac{M_{bc}}{\rho_{sb}} + \frac{M_{bc}}{\rho_{sb}(1-\phi_{bc})}\phi_{bc}(1-f) \tag{11}$$

If $f = 1$, (effective pore volume was the sum of interpore plus intrapore volume), the Eq. (11) simplifies to Eq. (8). If $f = 0$, (effective pore volume is interpore volume only), then Eq. (11) simplifies to Eq. (9).

If we reorganize Eq. (11), we obtain:

$$V_{bc} = \frac{M_{bc}}{\rho_{sb}}\left(1 + \frac{\phi_{bc}(1-f)}{1-\phi_{bc}}\right) = \frac{M_{bc}}{\rho_{sb}}\left(1 + \frac{(1-f)}{\frac{1}{\phi_{bc}} - 1}\right) \tag{12}$$

To calculate effective pore volume in Eq. (6), we substituted $\frac{M_s}{\rho_{ss}}$ for V_s (see Eq. (7)) and $\frac{M_{bc}}{\rho_{sb}}\left(1 + \frac{(1-f)}{\frac{1}{\phi_{bc}}-1}\right)$ for V_{bc} (see Eq. (12)). Then, Eq. (6) became Eq. (13):

$$V_{ep} = V_T - \frac{M_s}{\rho_{ss}} - \frac{M_{bc}}{\rho_{sb}}\left(1 + \frac{(1-f)}{\frac{1}{\phi_{bc}} - 1}\right) \tag{13}$$

By combing Eqs. (5) and (13), we obtained Eq. (14) for calculating effective porosity accessible to water in the biochar–sand mixture system.

$$\phi_{eff} = \frac{V_T - \frac{M_s}{\rho_{ss}} - \frac{M_{bc}}{\rho_{sb}}\left(1 + \frac{(1-f)}{\frac{1}{\phi_{bc}}-1}\right)}{V_T} = 1 - \frac{M_s}{\rho_{ss}V_T} - \frac{M_{bc}}{\rho_{sb}V_T}\left(1 + \frac{(1-f)}{\frac{1}{\phi_{bc}}-1}\right) \tag{14}$$

In Eq. (14), if $f = 0$, ϕ_{eff} was the interporosity of the mixture. If $f = 1$, $\phi_{eff} = \phi_T$ which was the sum of interporosity and intraporosity. To calculate ϕ_{eff} using Eq. (14), we measured M_s, ρ_{ss}, M_{bc}, ρ_{sb} and V_T; however ϕ_{bc} and f are two unknowns.

We assumed $\phi_{bc} = 0.622\ m^3/m^3$ for mesquite biochar produced at 400 °C based on the analysis of Brewer et al. (2014). In their paper, they calculated internal porosity of mesquite biochar produced at different temperatures from measured skeletal density data and envelope density data. Their biochar and our biochar were produced by the same technique.

The fraction (f) of biochar intraporosity that is accessible to water depends on the biochar surface chemistry, biochar internal pore size distribution, and biochar pore connectivity. If the biochar surface is hydrophilic ($\theta < 90°$) then water entry pressure is negative (Baker and Hillel, 1990). If these pores are connected and larger than a water molecule, water can enter the pores and $f = 1$, meaning the pores can all be filled with water. On the other hand, if the biochar is hydrophobic ($\theta > 90°$), then water entry pressure is positive (Wang et al., 2000). In this case, the water pressure needs to exceed the entry pressure in order for water to enter the biochar pores. As a result, for hydrophobic biochar, water fills up the big pores first followed by the small pores because big pores have a lower water entry pressure than that of small pores (Bauters et al., 2000). As the water-phase pressure increases (e.g., higher hydrostatic pressure), smaller pores become saturated (thus higher f).

The minimum biochar pore diameter (D) that can be invaded by water at certain hydrostatic pressure ($=\rho_w g h$, $h = 0.25$ m) was determined by Eq. (15).

$$D = \frac{4\gamma\cos\theta}{\rho_w g h} \tag{15}$$

where γ is interfacial tension between water and air at room temperature (0.072 N/m) and θ is the contact angle between the water–air interface and biochar surface.

Data on the contact angle for biochar is limited. We used $\theta = 120°$ in our calculation. This number was the maximum reported contact angle of biochar we found in existing studies (Herath et al., 2013; Smetanova et al., 2012; Wang et al., 2013). This contact angle corresponded to a breakthrough pore diameter of 59 μm for a hydrostatic pressure of 2.45 kPa (0.25 m of hydraulic head). Brewer et al. (2014) reported 12% ($f = 0.12$) of biochar pores were larger than 59 μm from mercury pore size distribution data of 450 °C mesquite biochar.

In the case when biochar is hydrophobic, there are some uncertainties in determining f. First, the hydrophobicity of biochar can be reduced by water treatment (Kinney et al., 2012) and then the contact angle of biochar may decrease. The decrease of contact angle would result in a decrease of breakthrough D and a corresponding increase of f. A second source of uncertainty was our use of the pore size distribution of mesquite biochar measured by mercury porosimetry from Brewer et al. (2014) to determine f. Because mercury porosimetry does not differentiate between interpores and intrapores, f might be slightly overestimated by this technique; however, for this mesquite biochar there was no statistical differences between mercury-determined porosity ($0.660\ m^3/m^3$) and He-determined porosity ($0.667 \pm 0.017\ m^3/m^3$) (Brewer et al., 2014).

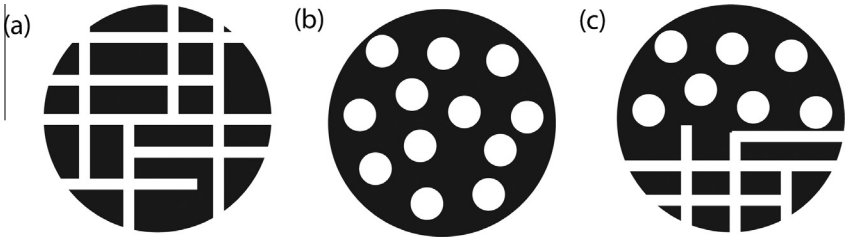

Fig. 2. Idealized, 2D biochar particles with internal (a) connected pores, (b) unconnected pores and (c) both connected and unconnected pores had different biochar volume (V_{bc}). (a). When biochar internal pores were connected, V_{bc} was the volume of biochar skeleton measured by helium pycnometry; (b). When biochar internal pores were unconnected, V_{bc} was the volume of biochar skeleton plus biochar internal pores; (c) when biochar particles had both connected and unconnected pores, V_{bc} was volume of biochar skeletal plus non-accessible biochar internal pores.

Table 4
Pearson correlation coefficients between hydraulic conductivity and bulk density, water saturation, total porosity, effective porosity, interporosity, intraporosity; between cumulative DOC and bulk density, water saturation, total porosity, effective porosity, interporosity, intraporosity.

Results	Flush #	ρ_b	S	ϕ_T	ϕ_{eff}	ϕ_{inter}	ϕ_{intra}
Concentration experiment							
K	All	0.99	0.98	−0.99	−0.90	−0.81	−1.00
Cumulative DOC	0	−0.89	−0.95	0.89	0.92	0.90	0.85
Cumulative DOC	1	−0.99	−0.97	0.99	0.89	0.79	1.00
Cumulative DOC	2	−0.99	−0.98	0.99	0.89	0.80	1.00
Cumulative DOC	3	−0.99	−0.98	0.99	0.90	0.80	1.00
Cumulative DOC	4	−0.99	−0.98	0.99	0.90	0.81	1.00
Cumulative DOC	5	−1.00	−0.98	0.99	0.91	0.82	1.00
Cumulative DOC	6	−1.00	−0.98	0.99	0.91	0.82	1.00
Particle size experiment							
K	All	0.42	0.98	−0.42	−0.17	−0.06	−0.43
Cumulative DOC	0	−0.43	−0.56	0.50	0.88	0.86	0.17
Cumulative DOC	1	−0.90	−0.84	0.91	0.61	0.40	0.81
Cumulative DOC	2	−0.87	−0.87	0.88	0.61	0.41	0.78
Cumulative DOC	3	−0.87	−0.90	0.88	0.53	0.31	0.81
Cumulative DOC	4	−0.85	−0.91	0.86	0.53	0.32	0.79
Cumulative DOC	5	−0.84	−0.92	0.85	0.52	0.32	0.77
Cumulative DOC	6	−0.83	−0.93	0.84	0.49	0.29	0.78

2.4.4. Dissolved organic carbon measurement

We collected leachate after the two-day saturation period (Flush 0). We also collected leachate after each flush (Flush 1–6). The leachate was massed (Fisher Scientific Accu 4202, USA) and filtered through pre-combusted glass fiber filters (Whatman, GF/F, 1825-025, UK) with a nominal pore size of 0.7 μm (Kolka et al., 2008; Wangersky, 1993). Filtered leachate samples were then refrigerated until DOC analyses could be performed (ASTM International, 2009; Cleveland et al., 2010) using a high temperature combustion total C analyzer (Shimadzu TOCvcsh, Kyoto, Japan). Sample replicates indicate a 0.06 mg/L precision for DOC.

2.5. Statistical analyses

Statistical comparisons of K and DOC in leachate between various concentrations, particle sizes, and controls (sand) were done using two-tailed t-tests. Differences were deemed significant at a p-value less than 0.05. We computed Pearson correlation coefficients (R) to assess the relationship between geometric mean of K of all flushes and ρ_b, S, ϕ_T, ϕ_{eff}, ϕ_{inter}, and ϕ_{intra} as well as the relationship between cumulative DOC for each flush and ρ_b, S, ϕ_T, ϕ_{eff}, ϕ_{inter}, and ϕ_{intra} (Table 4).

3. Results

3.1. Biochar concentration, particle size, and hydraulic conductivity

In our concentration experiment, hydraulic conductivity decreased with increasing biochar concentration. For instance, hydraulic conductivity decreased by an average of 72 ± 3% ($p < 0.001$) with biochar concentration of 10 wt% compared to pure sand (Fig. 3). Previous studies proposed linear relations between log(K) and clay content. Here we employed a similar approach by relating log(K) and biochar concentration:

$$\log(K) = -0.0541 \times \text{biochar}\% - 3.166 (R^2 = 0.9851,\ K \text{ in m/s}) \quad (16)$$

This empirical relation means that K, not log(K), decreased by a factor of 1.28 with each 2 wt% increase in biochar concentration. Any change in sand and biochar properties (i.e. particle size of sand and biochar, feedstock, pyrolysis temperature of biochar, hydrophobicity, intrapore size, and interpore size) would affect the slope and intercept of this relationship. Although this function was constrained for materials (particle size and surface chemistry) in our concentration experiment, it adds additional information on the magnitude of changes in K that can be expected from biochar. This expands our understanding of the physical processes controlling biochar effects on soil hydrology.

To understand the physical controls that drive K changes with biochar addition, we considered the effects of particle size. We determined that biochar particles finer than sand particles played an important role in decreasing K; biochar particles coarser than sand particles decreased K as well, but to a lesser extent (Fig. 3). At 2 wt% biochar rate, when biochar particles were finer than the sand particles, K of the mixture was 72 ± 2% lower than K of pure sand ($p < 0.001$). Hydraulic conductivity decreased by 15 ± 2% when the biochar particle size was coaser than the sand particle size ($p < 0.01$). When biochar and sand particle sizes were comparable, K was the same ($p = 0.25$) (Fig. 4).

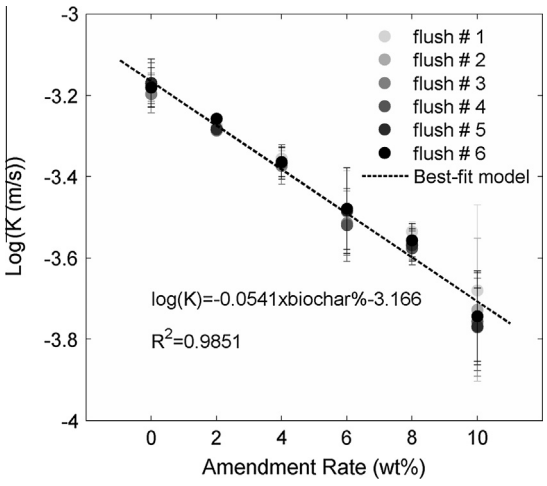

Fig. 3. Effects of biochar concentration on *K*. Hydraulic conductivity decreased as biochar rate increased from 0 to 10 wt%. The dashed line is an empirical, linear relationship between log(*K*) and biochar concentration (biochar%). Values and error bars were the average and standard deviation of three replicates conducted for each treatment.

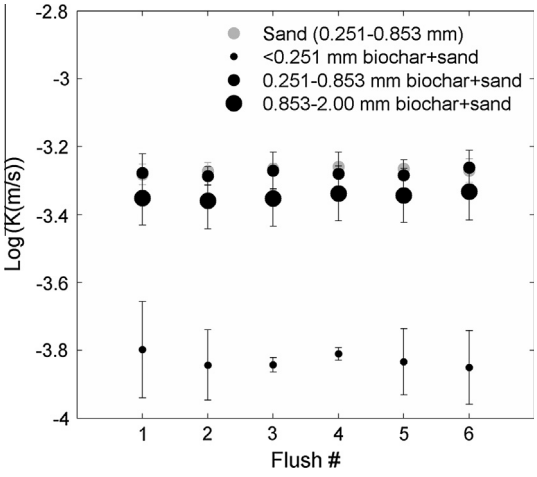

Fig. 4. Effects of biochar particle size on *K* at a biochar concentration of 2 wt%. Compared with the sand-only control (gray dots), fine biochar (<0.251 mm, small black dots) caused a significant decrease in *K*; when biochar particle size was equal to sand particle size (0.251–0.853 mm, medium black dots), no significant change in *K* was observed; larger biochar particles (0.853–2.00 mm, large black dots) than sand particles (0.251–0.853 mm) caused decrease of *K*. Values and error bars were the average and standard deviation of three replicates conducted for each treatment.

3.2. Skeletal density, bulk density, and water saturation

The biochar used in our concentration experiment had a lower skeletal density (1500 ± 10 kg/m^3) than the sand (2660 ± 20 kg/m^3, Table 2). For the biochar–sand mixtures, bulk density decreased from 1620 ± 30 kg/m^3 to 1110 ± 10 kg/m^3 from 0 to 10 wt% biochar rate. The final water saturation decreased from 102 ± 3% to 82 ± 5% when adding 10 wt% biochar (Table 3).

The skeletal density of biochar decreased with increasing particle size (1477 ± 2 kg/m^3, 1452 ± 5 kg/m^3, 1430 ± 5 kg/m^3 for fine, medium, and coarse biochar, respectively, Table 2). All biochar–sand mixtures (regardless of biochar particle size) had lower ρ_b (1540 ± 10 kg/m^3, 1520 ± 2 kg/m^3 and 1570 ± 10 kg/m^3 for fine, medium, and coarse biochar–sand mixtures, respectively) at a 2 wt% rate than those of pure sand (ρ_b: 1660 ± 40 kg/m^3, Table 3). The final water saturation of the sand-only and fine, medium, and coarse biochar–sand mixtures were 105 ± 5%, 88 ± 4%, 101 ± 1%, and 99 ± 3%, respectively.

3.3. Total porosity, effective porosity, interporosity, and intraporosity

Adding biochar into the system also changed the porosity of the sand–biochar mixtures. In the concentration experiment, ϕ_T, ϕ_{eff}, ϕ_{intra}, and ϕ_{inter} increased with biochar rate (Fig. 5a). For example, ϕ_T increased from 0.39 ± 0.01 m^3/m^3 to 0.55 ± 0.0 m^3/m^3 and ϕ_{intra} increased from 0 to 0.12 ± 0.0 m^3/m^3 from 0 to 10 wt% biochar. Effective porosity increased slightly from 0.39 ± 0.01 m^3/m^3 to 0.45 ± 0.0 m^3/m^3 and intraporosity increased slightly from 0.39 ± 0.01 m^3/m^3 to 0.43 ± 0.0 m^3/m^3 from 0 to 10 wt% biochar. Although we observed a generally increasing trend of interporosity and effective porosity with biochar concentration from 0 to 10 wt%, the change of interporosity and effective porosity is subtle for each 2 wt% increase of biochar concentration. As a result, we did not see big differences of interporosity and effective porosity between 4 wt % and 6 wt% biochar rate. They are statistically the same within error.

In our particle size experiment, biochar–sand mixtures had higher ϕ_T (0.41 ± 0.0 m^3/m^3, 0.42 ± 0.01 m^3/m^{3}and 0.40 ± 0.01 m^3/m^3 for fine, medium, and coarse biochar–sand mixtures, respectively) than pure sand (0.38 ± 0.02 m^3/m^3) (Fig. 5b). Biochar–sand mixtures had similar ϕ_{inter} (0.38 ± 0.0 m^3/m^3, 0.38 ± 0.01 m^3/m^3 and 0.37 ± 0.01 m^3/m^3 for fine, medium, and coarse biochar–sand mixtures, respectively) in comparison to pure sand (0.38 ± 0.02 m^3/m^3). Because only 12% of ϕ_{intra} was accessible to water (f = 0.12) and biochar rate was only 2 wt%, the ϕ_{eff} was slightly higher than ϕ_{inter} for biochar–sand mixtures.

3.4. Leaching of biochar C as DOC

To explore the fraction of biochar C lost through leachate as DOC, we analyzed effluent from each flush for DOC concentration and calculated mass loss of biochar C. In our concentration experiment, the cumulative DOC released from all seven flushes (Flush 0–6) increased from 1.4 ± 0.1 mg to 20 ± 1 mg (or increased by 1350%) from 0 to 10 wt% biochar (Fig. 6). The DOC mainly leached during Flush 1, which contributed 35%, 58%, 65%, 74%, 76% and 75% of the cumulative DOC loss for 0, 2, 4, 6, 8 and 10 wt% biochar, respectively. The percentages of total biochar C that moved as DOC (based on the mass of DOC observed and the known mass of biochar C added to the mixtures) were similar across all treatments: 0.18 ± 0.01 wt%, 0.16 ± 0.01 wt%, 0.15 ± 0.01 wt%, 0.14 ± 0.01 wt% and 0.14 ± 0.01 wt% for 2 wt%, 4 wt%, 6 wt%, 8 wt% and 10 wt% biochar treatments, respectively. The very low levels of DOC released from sand might come from the sand collection site or from the tap water (DOC concentration = 5.78 ± 0.08 mg/L) used during wet-sieving, or both.

In our particle size experiment, the cumulative DOC released from Flush 0 to Flush 6 decreased as biochar particle size increased (decreased by 46% from fine to coarse biochar–sand mixtures) (Fig. 7). Similar to the concentration experiment, the largest portion of the DOC came out in Flush 1, which contributed 61%, 70%, and 54% of the cumulative DOC mass loss for fine, medium, and coarse biochar–sand mixtures, respectively. The fraction of biochar C that moved as DOC was 0.15 ± 0.02 wt%, 0.08 ± 0.01 wt% and 0.06 ± 0.02 wt% of total biochar C added for fine, medium, and coarse biochar treatments, respectively.

4. Discussion

4.1. Hydrophobicity and pore characteristics as controls on hydraulic conductivity

Hydraulic conductivity correlates to soil properties like particle hydrophobicity, pore connectivity, pore size, and tortuosity

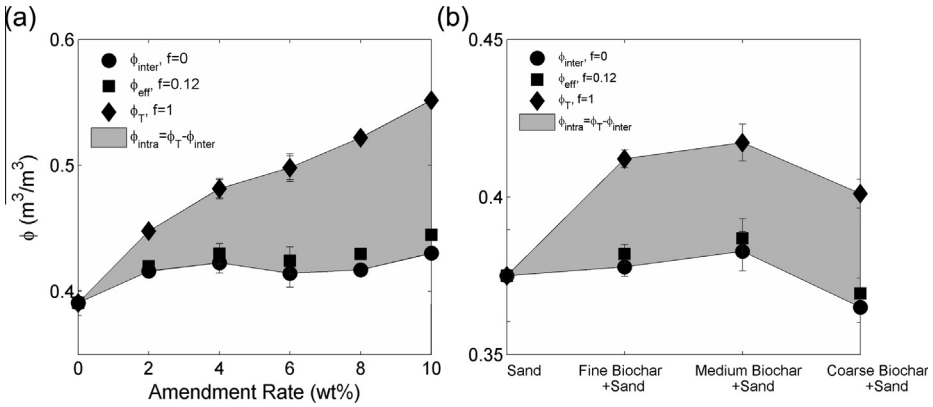

Fig. 5. Total porosity, effective porosity, interporosity and intraporosity of sand and biochar–sand mixtures. Adding biochar into sand increased total porosity and intraporosity in the system because biochar has intrapores. In our concentration experiment, not all biochar internal pores were accessible to water, and as a result, effective porosity was not equal to total porosity and it was slightly higher than interporosity (a). In our particle size experiment, interporosities of biochar–sand mixtures were similar to sand (b).

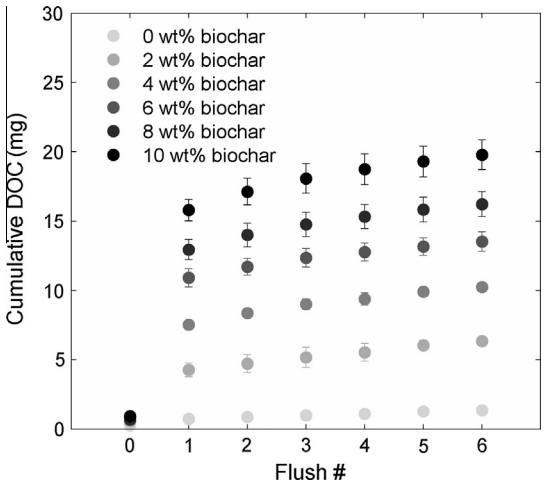

Fig. 6. Cumulative dissolved organic carbon (DOC; mg) through Flush 0–6 increased with biochar rate (0–10 wt%). The biochar particle size used in this experiment was <0.853 mm. Values and error bars were the average and standard deviation of three replicates conducted for each treatment.

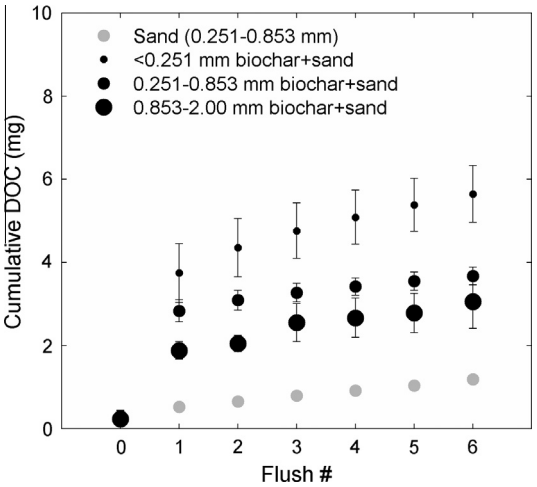

Fig. 7. Cumulative dissolved organic carbon (DOC; mg) through flushes increased as biochar particle size decreased at 2 wt% biochar rate. Values and error bars were the average and standard deviation of three replicates conducted for each treatment.

(Carman, 1937; Kozeny, 1927). Our biochars were slightly hydrophobic (MED index = 3–5; Table 1) and all biochar–sand mixtures were hydrophilic (MED index = 0, Table 1). The difference between hydrophobic biochar and hydrophylic biochar–sand mixtures indicate that this type of biochar did not cause major change in bulk hydrophobicity of biochar–sand mixtures at the concentrations we examined (0–10 wt%). However, the hydrophobicity of biochar particles, or biochar's small intrapore size, or both, may cause a high intrapore entry pressure, which prevented water from penetrating intrapores. For instance, our estimation showed that total porosity increased more than effective porosity (Fig. 5). In our biochar concentration experiments total porosity increased by 0.16 m^3/m^3 and effective porosity increased by 0.06 m^3/m^3 from 0 wt% to 10 wt% biochar rate. This is likely because the applied hydraulic pressure (0.25 m of water) at the beginning of falling head experiment was not enough to overcome the entry pressure caused by the hydrophobicity of biochar particle or biochar's small intrapore size, or both. Therefore, the increase of total porosity by adding biochar may not have been effective for water flow, and thus had little effect on *K*. Although biochar did not change the bulk hydrophobicity of the biochar–sand mixture at the low mass fraction in our experiments, it may affect flow at the pore scale. However, previous experimental and modeling studies showed that clay started to affect hydraulic conductivity at volume fraction as low as 5% (Daigle and Reece, 2015; Revil and Cathles, 1999). Similarly, we speculate that these individual biochar particles can interact with water in sand thus have impact on properties such as *K* but not drive a major change in hydrophobicity.

Biochar intrapore connectivity may be affected by grinding and also may be related to pore size. When intrapores are not connected, they act as isolated pockets of gas, creating an apparent skeletal density that is lower than the true skeletal density (Fig. 8b, left). The lower ρ_{sb} of the coarse biochar (Table 2) reflected the preservation of isolated, unconnected pores. Grinding biochar into finer size particles opened the unconnected intrapores (Fig. 8b, right) and allowed He to enter. As a result, the finer biochar particles had a higher skeletal density as determined by He pycnometry. However, water moved faster in larger pores than in smaller pores when pores were saturated and thus larger pores dominated water flow when pores were connected. For instance, when biochar and sand particles of the same particle size were mixed at 2 wt% biochar, the biochar–sand mixture had the same ϕ_{inter} (0.38 ± 0.01 m^3/m^3) to that of pure sand (0.38 ± 0.01 m^3/m^3). Meanwhile, the *K* values of these two treatments were the same (p = 0.25) and the treatments were fully saturated (Table 3). In

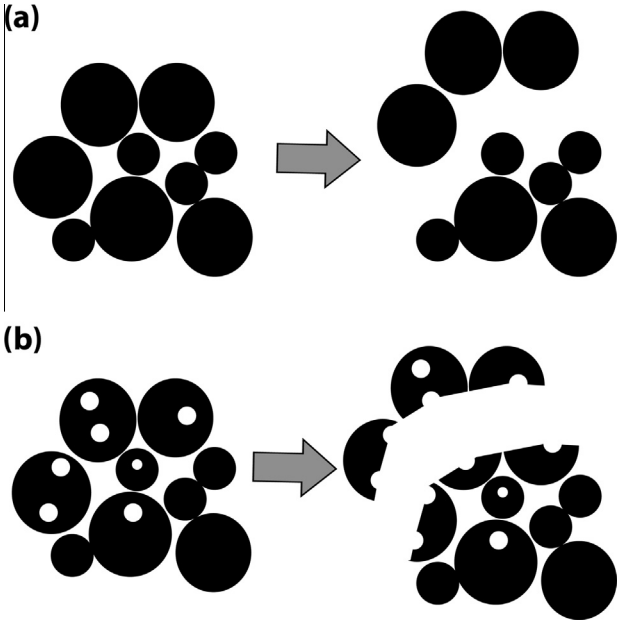

Fig. 8. Illustration showing how biochar's skeletal density (ρ_{sb}) may change after grinding (from left to right) soil aggregates with (a) solid particles and (b) particles with isolated intrapores. (a) Skeletal density did not change by breaking (white bar) soil particle aggregates; ρ_{sb} was identical in the single aggregate (left) and as in the broken aggregate (two pieces) (right). (b) After grinding particles with isolated pores, He can access these pores, increasing ρ_{sb} as determined by He pycnometry.

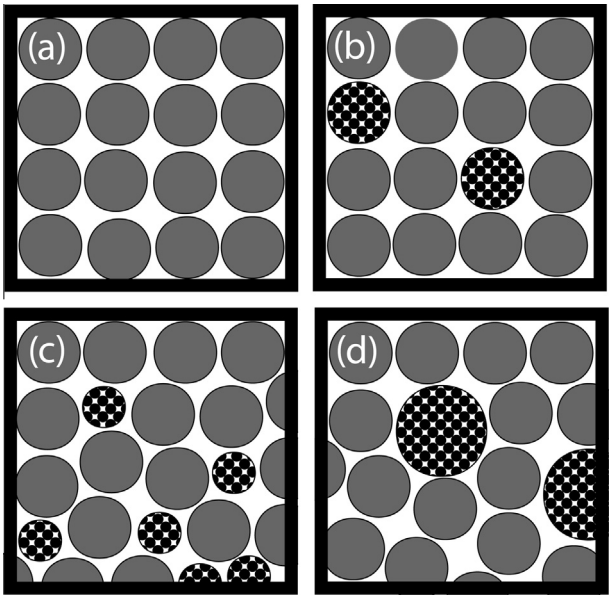

Fig. 9. Illustration showing idealized mixture of pure sand (gray circles) and biochar (circles with black pattern). (a) particle arrangement of sand as control, (b) particle arrangement was the same when biochar and sand particles are of the same size, (c) fine biochar particles filled in the pores between sand particles resulting in more compacted packing than control thus reduced porosity and increased tortuosity, (d) sand particles surrounding big biochar particles increased tortuosity.

addition, the Pearson correlation coefficients (R) between K and ϕ_T, ϕ_{eff}, ϕ_{inter}, and ϕ_{intra} were −0.99, −0.90, −0.81 and −1.00 in concentration experiments and were −0.42, −0.17, −0.06 and −0.43 in particle size experiments, respectively (Table 4). This negative correlation between K and porosity indicates that the increase of porosity by introducing biochar intrapores is not necessarily providing flow paths for water, and thus does not have a positive effect on K. Therefore, it is likely that the smaller intrapores were poorly hydraulically connected and larger interpores dominated the flow path (Fig. 9b).

Our results showed that mixing sand with biochar of different particle sizes can change interpore size and tortuosity. When biochar particles were finer than sand particles, the biochar particles filled the pores between the sand particles, resulting in more effective packing (Fig. 9c) and higher bulk density (Table 3) than when biochar particles were the same size as the sand particles (both under the same compaction force). This reduced intergranular pore throat size and increased tortuosity. If interpores dominated water flow (as we hypothesize), the geometric changes to the interpores caused by adding finer biochar particles may have accounted for the observed reduction in K (Fig. 4).

When biochar particles were coarser than sand particles, sand particles likely surrounded biochar particles (Fig. 9d), which may explain the higher bulk density (Table 3) in this case compared to mixtures where biochar and sand particles were of the same size. The denser packing caused by coarser biochar may also decrease pore throat size between particles and increase tortuosity. If interpores dominated water flow, these changes of interpores due to addition of coarser biochar particles can explain the observed reduction in K (Fig. 4).

4.2. Implications for field application

Biochar application methods can affect the distribution of biochar in soil, with concomitant effects on soil K. In our experiments we mixed biochar with sand uniformly, which most closely represents uniform topsoil mixing conditions. Other application methods such as top dressing or deep-banding into the rhizosphere (Lehmann and Joseph, 2009) may create heterogeneous biochar–sand mixtures, resulting in different effects on K compared with uniform mixing. For example, when adding fine biochar particles, the vertical K of deep-banded soils will be even lower than that of uniformly mixed soils because finer biochar particles would create a low permeability layer causing water to preferentially move horizontally.

In addition, it is important to consider temporal changes in K of biochar–soil mixtures. For example, coarse biochar particles can be broken into finer-sized particles by plant roots and other natural forces such as freeze–thaw cycles (Lehmann and Joseph, 2009; Spokas et al., 2014). As biochar particle size decreases, we anticipate that K will also decrease as observed in our experiments. Additionally, biochar may change soil K by changing plant physical properties, like root size and density, as previous studies have shown that biochar application can increase rice root diameter (Noguera et al., 2010), which may increase the diameter of soil macropores (Hu et al., 2015) and result in increased K.

It is also important to consider local ionic strength in the field. Biochar has a higher mobility in water with a lower ionic strength than in water with a higher ionic strength (Zhang et al., 2010). We used low ionic strength water in our experiment; thus biochar is more susceptible to be transported. In some cases, transported biochar may then form clogs in pores and reduce K. Biochar can also act as a source of cations to the solution resulting in an increase of ionic strength. The increase may cause a decrease in DOC concentration (Hruska et al., 2009) and then DOC may have less effect on K. Although we did not observe the effect of this negative feedback (between DOC and ionic strength) on K in biochar–sand mixtures at laboratory scale, this may occur over long residence times or more water flushing events.

Biochar concentration, biochar/soil particle size distribution (soil texture), and application techniques should be considered together to evaluate the most effective application scenario for the desired field conditions. We also need to consider changes in

water storage and K of biochar–soil mixtures when defining an optimal biochar application rate and particle size to maximize water retention without adversely affecting water flow. To reduce water drainage in sandy areas, biochar particles that are finer than soil particles may be more effective (Fig. 4). However, finer biochar particles may introduce more DOC leaching to groundwater compared to coarser biochar particles (Fig. 7), although our data suggest that the overall effect of biochar on DOC fluxes is likely to be minor. In addition, during application particles less than 2.5 μm may enter the atmosphere and become part of the $PM_{2.5}$ pool, adversely affecting human health (WHO Europe, 2003) and climate (IPCC, 2003). This risk points to the need for application techniques that deliver biochar particles into the soil without introducing particles into atmosphere. Ideally biochar would be broken down into desired particle sizes only once in the soil. To reduce groundwater pollution caused by biochar-induced DOC leaching, pretreatment of biochar to remove leachable C may sometimes be needed, depending on the chemistry of the biochar used.

Our experiments suggest that biochar's effect on soil K was mainly controlled by interparticle space (interpores). When biochar particles are finer than sand particles, finer biochar filled interpores between sands resulting in a creation of smaller pores and an increase of tortuosity, thus decreasing K. Based on this theory, we expect that biochar with low intraporosity (e.g., poultry litter) would likely also reduce soil K if biochar particles were finer than soil particles. While biochar particles in this study were relatively monodisperse, other studies with polydisperse particles have shown similar results. Brockhoff et al. (2010) reported a decrease in K in a sandy soil when fast pyrolysis switchgrass biochar was used. This switchgrass had a very fine particle size, with approximately 20 wt%, 30 wt%, and 50 wt% of the particles coarser than 100 μm, between 50 and 100 μm, and finer than 50 μm, respectively (Brewer, unpublished data).

When biochar particles (0.853–2.00 mm) were slightly coarser than sand particles (0.251–0.853 mm), biochar caused a 15 ± 2% decrease in K. It is possible that this effect may not persist when adding coarser biochar into soil with finer textures (e.g. clay or silt). Indrawan et al. (2006) found that permeability of a clayey sand was increased by mixing with either a gravelly sand or a medium sand by developing large pores between particles. Similarly, when biochar particles become much coarser than soil particles, it may be that much coarser biochar particles increase the size of pores between particles, driving an overall increase in K. For instance, Barnes et al. (2014) found that adding mesquite biochar (50 wt% of biochar particle >0.32 mm) increased the K of clay by 328%. Herath et al. (2013) observed an increase in K by 32% and 139% when adding 350 °C corn stover biochar (88 wt% of biochar particle >0.25 mm) and 550 °C corn stover biochar (92 wt% of biochar particle >0.25 mm) into Alfisols (silt loam). Herath et al. (2013) also showed that K of Alfisols (silt loam) increased by 50% for unpyrolyzed corn stover (coarser than corn stover biochar). This suggested that biochar may behave similarly to fresh organic material in influencing soil K.

4.3. Implications for soil water storage

Biochar application may increase soil porosity by introducing a significant volume of nanometer-sized intrapores (<2 nm) inside of biochar particles (Sun et al., 2012). These intrapores may be beneficial for plant growth by increasing soil water storage. However, these intrapores may be accessible to helium but not water because He molecules are smaller and less viscous than water molecules; as a result, the He measurements provide an upper limit of pore space (or ϕ_T).

Our effective porosity calculation estimated pore space that was accessible to water. The lower effective porosity compared to total porosity for biochar-amended sand explains the observed partial saturation when saturation is defined based on helium pycnometry measurements. In our concentration experiment, S decreased with increasing biochar concentration (Table 3). In the particle size experiment, samples with finer biochar particles were not fully saturated (Table 3). In addition, all sand samples but not all biochar–sand mixtures were fully saturated. This suggested that the hydrostatic pressure in our experiment was not high enough to exceed the water entry pressure of some of the biochar intrapores due to biochar's hydrophobicity. This observation leads us to speculate that some biochar intrapores might be too small to be invaded by water once biochar is applied near surface. If ponding water pressure is not high enough to overcome water entry pressure of smaller intrapores, biochar intrapores might not be fully saturated. However, this partial saturation of biochar is unlikely to significantly reduce its water storage benefits because these nanopores are a small fraction of total biochar porosity (but only for plant-derived chars) (Brewer et al., 2014).

The effect of biochar on soil water storage could also vary with soil texture and biochar type. Previous studies summarized by Masiello et al. (2015) suggested that biochar either increased or caused no significant change in water storage, and the improvement of soil water storage was largest in soils with lower water storage capacity (i.e. sandy soil). For example, hardwood biochar added to a sandy soil caused the largest change in water storage (Novak et al., 2012).

4.4. Implications for C sequestration

We found that only a small portion of biochar C moved as DOC. These findings are consistent with previous studies that reported minimal DOC leaching from biochar-amended field plots (Bell and Worrall, 2011; Major et al., 2010). Most of the DOC was lost during the first flush, suggesting that the majority of leachable C may be removed during the first rain event after the biochar amendment. Once in the field, biochar can be microbially decomposed (Baldock and Smernik, 2002) and physically broken down by processes like freezing and thawing, tillage, or bioturbation (Spokas et al., 2014). Decayed biochar C dissolved in water leads to further leaching of DOC. Given that more DOC and a greater fraction of biochar C was lost as DOC from the finer biochar particles (Fig. 7), physical and/or chemical weathering of biochar could lead to further DOC loss due to increase of biochar surface area in contact with water. In field applications, precipitation of iron hydroxides at the oxic surface layer can remove some DOC thus reducing DOC leaching (Riedel et al., 2013). The Pearson correlation coefficients between DOC and ϕ_T, ϕ_{eff}, ϕ_{inter} and ϕ_{intra} were 0.89 to 0.99, 0.89 to 0.92, 0.79 to 0.90 and 0.85 to 1.00 for all flushes in concentration experiments and were 0.50 to 0.91, 0.49 to 0.88, 0.29 to 0.86 and 0.17 to 0.81 for all flushes in particle size experiments, respectively. Meanwhile, the Pearson coefficients between DOC and ρ_b were −1.00 to −0.89 for all flushes in concentration experiments and were −0.90 to −0.43 for all flushes in particle size experiments, respectively (Table 4). The positive correlation between DOC and porosities and negative correlation between DOC and ρ_b suggest that biochar carbon is more susceptible to be transported as DOC in less dense and more pore space media.

Biochar's effect on DOC leaching has also been shown to vary with soil texture. Barnes et al. (2014) observed that DOC leaching either increased, decreased, or did not change depending on the type of soil. Increases in DOC leaching were observed when adding biochar into C-poor sand, decreases in DOC leaching were observed when adding biochar to C-rich organic soil, and no change was observed when biochar was mixed to a clay-rich soil. This

suggested that while biochar can add leachable C to the soil, it is also capable of absorbing soil-derived C.

5. Conclusions

The hydraulic conductivity (K) of sand varied with biochar concentration and also with biochar particle size. Hydraulic conductivity decreased by 72 ± 3% as biochar content increased from 0 to 10 wt%. For a 2 wt% biochar, K decreased by 72 ± 2% when biochar particles were finer than sand particles. In our concentration experiment, despite higher total porosity (ϕ_T), the K of our biochar–sand mixture was the same as that of pure sand, indicating that intrapores (pores inside of biochar particles) accessed by helium may not be hydraulically connected or accessible by water. The decrease of K following the addition of finer biochar particles was likely the result of increased tortuosity and reduced pore throat sizes in the mixture. The decrease of K associated with larger biochar particles was likely caused by the bimodal particle size distribution in the sand–biochar mixture, resulting in denser packing and increased tortuosity. Although the DOC in the leachate increased with biochar concentration (by 1350% at 10 wt% biochar) and decreased as particle size increased, only 0.06–0.18 wt% of biochar C was transported as DOC for all experiments. Over the long term, effects of microbial activity, soil aggregation and climate on biochar may alter biochar's impact on soil hydraulic conductivity and C mobility.

Acknowledgements

This work was supported by US NSF EAR-0911685. We thank K. Ziegelgruber for help measuring DOC, T. Giachetti, L. Driver, V. Chuang and C. Nguyen for assistance with skeletal density measurements, X.D. Gao and K. Hodge for help conducting EA measurements, and T.J. Kinney and C. LeCroy for assistance on methods for producing biochar. We thank five anonymous reviewers for their insightful comments, which helped us to improve the manuscript.

References

ASTM International, 2006. Standard Test Method for Permeability of Granular Soils (Constant Head) (Standard D2434). American Society for Testing and Materials, West Conshohocken, PA. http://dx.doi.org/10.1520/D2434-68R06.

ASTM International, 2009. Standard Test Method for Total Carbon and Organic Carbon in Water by High Temperature Catalytic Combustion and Infrared Detection (D7573). American Society for Testing and Materials, West Conshohocken, PA. http://dx.doi.org/10.1520/D7573-09.

ASTM International, 2010. Standard Test Methods for Measurement of Hydraulic Conductivity of Saturated Porous Materials Using a Flexible Wall Permeameter. American Society for Testing and Materials, West Conshohocken, PA. http://dx.doi.org/10.1520/D5084-10.

Baker, R.S., Hillel, D., 1990. Laboratory tests of a theory of fingering during infiltration into layered soils. Soil Sci. Soc. Am. J. 54 (1), 20–30. http://dx.doi.org/10.2136/sssaj1990.03615995005400010004x.

Baldock, J.A., Smernik, R.J., 2002. Chemical composition and bioavailability of thermally altered *Pinus resinosa* (red pine) wood. Org. Geochem. 33, 1093–1110. http://dx.doi.org/10.1016/S0146-6380(02)00062-1.

Barnes, R.T., Gallagher, M.E., Masiello, C.A., Liu, Z., Dugan, B., 2014. Biochar-induced changes in soil hydraulic conductivity and dissolved nutrient fluxes constrained by laboratory experiments. PLOS ONE.

Bauters, T.W.J. et al., 2000. Physics of water repellent soils. J. Hydrol. 231, 233–243. http://dx.doi.org/10.1016/s0022-1694(00)00197-9.

Bell, M.J., Worrall, F., 2011. Charcoal addition to soils in NE England: a carbon sink with environmental co-benefits? Sci. Total Environ. 409, 1704–1714. http://dx.doi.org/10.1016/j.scitotenv.2011.01.031.

Brewer, C.E. et al., 2014. New approaches to measuring biochar density and porosity. Biomass Bioenergy. http://dx.doi.org/10.1016/j.biombioe.2014.03.059.

Brockhoff, S.R., Christians, N.E., Killorn, R.J., Horton, R., Davis, D.D., 2010. Physical and mineral-nutrition properties of sand-based turfgrass root zones amended with biochar all rights reserved. No part of this periodical may be reproduced or transmitted in any form or by any means, electronic or mechanical, including photocopying, recording, or any information storage and retrieval system, without permission in writing from the publisher. Agron. J. 102 (6), 1627–1631. http://dx.doi.org/10.2134/agronj2010.0188.

Carman, P.C., 1937. Fluid flow through granular beds. T. I. Chem. Eng-Lond 15, 150–166.

Cleveland, C.C., Wieder, W.R., Reed, S.C., Townsend, A.R., 2010. Experimental drought in a tropical rain forest increases soil carbon dioxide losses to the atmosphere. Ecology 91 (8), 2313–2323. http://dx.doi.org/10.1890/09-1582.1.

Czimczik, C., Masiello, C.A., 2007. Controls on black carbon storage in soils. Glob. Biogeochem. Cycl. 21, GB3005. http://dx.doi.org/10.1029/2006GB002798.

Daigle, H., Reece, J., 2015. Permeability of two-component granular materials. Transp. Porous Med. 106 (3), 523–544. http://dx.doi.org/10.1007/s11242-014-0412-6.

Deal, C., Brewer, C.E., Brown, R.C., Okure, M.A.E., Amoding, A., 2012. Comparison of kiln-derived and gasifier-derived biochars as soil amendments in the humid tropics. Biomass Bioenergy 37, 161–168.

Dittmar, T. et al., 2012. Continuous flux of dissolved black carbon from a vanished tropical forest biome. Nat. Geosci. 5, 618–622. http://dx.doi.org/10.1038/NGEO1541.

Doerr, S.H., 1998. On standardizing the water drop penetration time and the molarity of an ethanol droplet techniques to classify soil hydrophobicity: a case study using medium textured soils. Earth Surf. Process. Landforms 23, 663–668.

Foereid, B., Lehmann, J., Major, J., 2011. Modeling black carbon degradation and movement in soil. Plant Soil 345, 223–236. http://dx.doi.org/10.1007/s11104-011-0773-3.

Freeze, R.A., Cherry, J.A., 1979. Groundwater. Prentice-Hall Inc., Englewood Cliffs, NJ.

Githinji, L., 2013. Effect of biochar application rate on soil physical and hydraulic properties of a sandy loam. Arch. Agron. Soil Sci. 1–14. http://dx.doi.org/10.1080/03650340.2013.821698.

Githinji, L., 2014. Effect of biochar application rate on soil physical and hydraulic properties of a sandy loam. Arch. Agron. Soil Sci. 60 (4), 457–470. http://dx.doi.org/10.1080/03650340.2013.821698.

Glaser, B., Lehmann, J., Zech, W., 2002. Ameliorating physical and chemical properties of highly weathered soils in the tropics with charcoal – a review. Biol. Fertil. Soils 35, 219–230. http://dx.doi.org/10.1007/s00374-002-0466-4.

Herath, H.M.S.K., Camps-Arbestain, M., Hedley, M., 2013. Effect of biochar on soil physical properties in two contrasting soils: an Alfisol and an Andisol. Geoderma 209–210, 188–197. http://dx.doi.org/10.1016/j.geoderma.2013.06.016.

Hockaday, W.C., Granna, A.M., Kim, S., Hatcher, P.G., 2006. Direct molecular evidence for the degradation and mobility of black carbon in soils from ultrahigh-resolution mass spectral analysis of dissolved organic matter from a fire-impacted forest soil. Org. Geochem. 37, 501–510. http://dx.doi.org/10.1016/j.orggeochem.

Hruška, J., Krám, P., McDowell, W.H., Oulehle, F., 2009. Increased Dissolved Organic Carbon (DOC) in Central European streams is driven by reductions in ionic strength rather than climate change or decreasing acidity. Environ. Sci. Technol. 43 (12), 4320–4326. http://dx.doi.org/10.1021/es803645w.

Hu, X., Li, Z.C., Li, X.Y., Liu, Y., 2015. Influence of shrub encroachment on CT-measured soil macropore characteristics in the Inner Mongolia grassland of northern China. Soil Till. Res. 150, 1–9. http://dx.doi.org/10.1016/j.still.2014.12.019.

IBI, 2013. Standardized Product Definition and Product Testing Guidelines for Biochar That is Used in Soil (International Biochar Initiative).

Indrawan, I.G.B., Rahardjo, H., Leong, E.C., 2006. Effects of coarse-grained materials on properties of residual soil. Eng. Geol. 82 (3), 154–164. http://dx.doi.org/10.1016/j.enggeo.2005.10.003.

IPCC, 2003. Climate Change 2001, IPCC, Online.

Jaffé, R. et al., 2013. Global charcoal mobilization from soils via dissolution and riverine transport to the oceans. Science 340 (6130), 345–347. http://dx.doi.org/10.1126/science.1231476.

Kinney, T.J. et al., 2012. Hydrologic properties of biochars produced at different temperatures. Biomass Bioenergy 41, 34–43. http://dx.doi.org/10.1016/j.biombioe.2012.01.033.

Klute, A., 1986. Methods of Soil Analysis, Part 1: Physical and Mineralogical Methods American Society of Agronomy, W.I. http://dx.doi.org/10.1002/gea.3340050110.

Kolka, R., Weishampel, P., Fröberg, M., 2008. Measurement and importance of dissolved organic carbon. In: Hoover, C. (Ed.), Field Measurements for Forest Carbon Monitoring. Springer, Netherlands, pp. 171–176. http://dx.doi.org/10.1007/978-1-4020-8506-2_13.

Kozeny, J., 1927. Über kapillare Leitung des Wassers im Boden. Akad. Wiss. Wien 136, 271–306.

Kuzyakov, Y., Subbotina, I., Chen, H., Bogomolova, I., Xu, X., 2009. Black carbon decomposition and incorporation into soil microbial biomass estimated by ^{14}C labeling. Soil Biol. Biochem. 41, 210–219.

Lehmann, J., Joseph, S., 2009. Biochar for Environmental Management: Science and Technology. Earthscan, UK.

Liu, J. et al., 2012. Short-term effect of biochar and compost on soil fertility and water status of a Dystric Cambisol in NE Germany under field conditions. J. Plant Nutr. Soil Sci. 175 (5), 698–707. http://dx.doi.org/10.1002/jpln.201100172.

Liu, X.Y. et al., 2013. Biochar's effect on crop productivity and the dependence on experimental conditions – a meta-analysis of literature data. Plant Soil 373 (1–2), 583–594. http://dx.doi.org/10.1007/s11104-013-1806-x.

Major, J., Lehmann, J., Rondon, M., Goodale, C., 2010. Fate of soil-applied black carbon: downward migration, leaching and soil respiration. Glob. Change Biol. 16, 1366–1379. http://dx.doi.org/10.1111/j.1365-2486.2009.02044.x.

Major, J., Steiner, C., Downie, A., Lehmann, J., 2009. Biochar Effects on Nutrient Leaching, Biochar for Environmental Management: Science and Technology. Earthscan, London, UK, pp. 271–288.
Masiello, C. et al., 2015. Biochar effects on soil hydrology. In: Lehmann, J., Joseph, S. (Eds.), Book Chapter.
Molina, M. et al., 2009. Reducing abrupt climate change risk using the Montreal Protocol and other regulatory actions to complement cuts in CO_2 emissions. Proc. Natl. Acad. Sci., USA 206, 1–6. http://dx.doi.org/10.1073/pnas.0902568106.
Noguera, D. et al., 2010. Contrasted effect of biochar and earthworms on rice growth and resource allocation in different soils. Soil Biol. Biochem. 42, 1017–1027. http://dx.doi.org/10.1016/j.soilbio.2010.03.001.
Novak, J.M. et al., 2012. Biochars impact on soil-moisture storage in an Ultisol and two Aridisols. Soil Sci. 177 (5), 310Y320. http://dx.doi.org/10.1097/SS.0b013e31824e5593.
Revil, A., Cathles, L., 1999. Permeability of shaly sands. Water Resour. Res. 35 (3), 651–662.
Riedel, T., Zak, D., Biester, H., Dittmar, T., 2013. Iron traps terrestrially derived dissolved organic matter at redox interfaces. Proc. Natl. Acad. Sci., USA 110 (25), 10101–10105. http://dx.doi.org/10.1073/pnas.1221487110.
Rumpel, C., Ba, A., Darboux, F., Chaplot, V., Planchon, O., 2009. Erosion budget and process selectivity of black carbon at meter scale. Geoderma 154, 131–137. http://dx.doi.org/10.1016/j.geoderma.2009.10.006.
Rumpel, C. et al., 2006. Preferential erosion of black carbon on steep slopes with slash and burn agriculture. Catena 65, 30–40. http://dx.doi.org/10.1016/j.catena.2005.09.005.
Schaetzl, R.J., 2002. A spodosol–entisol transition in northern Michigan. Soil. Sci. Soc. Am. J. 66, 1272–1284. http://dx.doi.org/10.2136/sssaj2002.1272.
Smetanova, A., Dotterweich, M., Diehl, D., Ulrich, U., Fohrer, N., 2012. Influence of biochar and terra preta substrates on wettability and erodibility of soils. Zeitschrift Fur Geomorphol. 57, 111–134. http://dx.doi.org/10.1127/0372-8854/2012/s-00117.
Spokas, K.A. et al., 2014. Physical disintegration of biochar: an overlooked process. Environ. Sci. Technol. Lett. 1 (8), 326–332. http://dx.doi.org/10.1021/ez500199t.
Streubel, J.D. et al., 2011. Influence of contrasting biochar types on five soils at increasing rates of application. Soil Biol. Biochem. 75, 1402–1413. http://dx.doi.org/10.2136/sssaj2010.0325.
Sun, H., Hockaday, W.C., Masiello, C.A., Zygourakis, K., 2012. Multiple controls on the chemical and physical structure of biochars. Ind. Eng. Chem. Res. 51, 3587–3597. http://dx.doi.org/10.1021/ie201309r.
Tryon, E.H., 1948. Effect of charcoal on certain physical, chemical, and biological properties of forest soils. Ecol. Monogr. 18 (1), 81–115. http://dx.doi.org/10.2307/1948629.
Wang, D., Zhang, W., Hao, X., Zhou, D., 2013. Transport of biochar particles in saturated granular media: effects of pyrolysis temperature and particle size. Environ. Sci. Technol. 47, 821–828. http://dx.doi.org/10.1021/es303794d.
Wang, Z., Wu, L., Wu, Q.J., 2000. Water-entry value as an alternative indicator of soil water-repellency and wettability. J. Hydrol. 231, 76–83. http://dx.doi.org/10.1016/s0022-1694(00)00185-2.
Wangersky, P.J., 1993. Dissolved organic carbon methods: a critical review. Mar. Chem. 41 (1–3), 61–74. http://dx.doi.org/10.1016/0304-4203(93)90106-X.
WHO Europe, 2003. Health Aspects of Air Pollution with Particulate Matter, Ozone and Nitrogen Dioxide Bonn, Germany.
Woolf, D., Amonette, J.E., Street-Perrott, F.A., Lehmann, J., Joseph, S., 2010. Sustainable biochar to mitigate global climate change. Nat. Commun. 1 (56), 1–9. http://dx.doi.org/10.1038/ncomms1053.
Zhang, W. et al., 2010. Transport and retention of biochar particles in porous media: effect of pH, ionic strength, and particle size. Ecohydrology 3, 497–508. http://dx.doi.org/10.1002/eco.160.
Zimmerman, A., 2010. Abiotic and microbial oxidation of laboratory-produced black carbon (biochar). Environ. Sci. Technol. 44, 1295–1301. http://dx.doi.org/10.1021/es903140c.